



Deposited via The University of Sheffield.

White Rose Research Online URL for this paper:

<https://eprints.whiterose.ac.uk/id/eprint/105121/>

Version: Accepted Version

Article:

Krynkin, A., Horoshenkov, K.V. and Van Renterghem, T. (2016) An airborne acoustic method to reconstruct a dynamically rough flow surface. *Journal of the Acoustical Society of America*, 140 (3). pp. 2064-2073. ISSN: 0001-4966

<https://doi.org/10.1121/1.4962559>

Reuse

Items deposited in White Rose Research Online are protected by copyright, with all rights reserved unless indicated otherwise. They may be downloaded and/or printed for private study, or other acts as permitted by national copyright laws. The publisher or other rights holders may allow further reproduction and re-use of the full text version. This is indicated by the licence information on the White Rose Research Online record for the item.

Takedown

If you consider content in White Rose Research Online to be in breach of UK law, please notify us by emailing eprints@whiterose.ac.uk including the URL of the record and the reason for the withdrawal request.

1 **An airborne acoustic method to reconstruct a dynamically rough flow**
2 **surface**

3 Anton Krynkin¹, Kirill V. Horoshenkov
4 Department of Mechanical Engineering, University of Sheffield,
5 Sheffield, S1 3JD, UK

6 Timothy Van Renterghem
7 Department of Information Technology, Ghent University, St.-Pietersnieuwstraat
8 41, 9000 Gent, Belgium

¹e-mail: a.krynkin@sheffield.ac.uk

Abstract

10 Currently, there is no airborne in-situ method to reconstruct with high
11 fidelity the instantaneous elevation of a dynamically rough surface of a turbu-
12 lent flow. This work proposes a new holographic method that reconstructs the
13 elevation of a 1-D rough water surface from airborne acoustic pressure data.
14 This method can be implemented practically using an array of microphones
15 deployed over a dynamically rough surface or using a single microphone which
16 is traversed above the surface at a speed that is much higher than the phase
17 velocity of the roughness pattern. In this work, the theory is validated using
18 synthetic data calculated with the Kirchhoff approximation and a finite dif-
19 ference, time domain method over a number of measured surface roughness
20 patterns. The proposed method is able to reconstruct the surface elevation
21 with a sub-millimetre accuracy and over a representatively large area of the
22 surface. Since it has been previously shown that the surface roughness pattern
23 reflects accurately the underlying hydraulic processes in open channel flow (e.g.
24 [Horoshenkov, et al, J. Geoph. Res.,118(3), 18641876 (2013)]), the proposed
25 method paves the way for the development of new non-invasive instrumen-
26 tation for flow mapping and characterization that are based on the acoustic
27 holography principle.

28 PACS: 43.20.Ye, 43.30.Hw, 43.28.Gq

29 Keywords: Acoustic scattering, roughness, dynamic surface, inverse method

30 I Introduction

31 Understanding the spatial and temporal hydraulic changes in rivers and other types
32 of open channels is of paramount importance for predicting flood risk, sediment
33 movement and consequent morphological change. Understanding the spatial and
34 temporal variability of flows has become a core element in assessing the water quality
35 and ecological status of rivers (EU Water Framework Directive (WFD)). However,
36 there is a significant shortcoming in our ability to monitor these flows at sufficient
37 temporal and spatial resolution particularly during extreme events because there is
38 no technology that can be deployed rapidly to accurately map the hydraulic and
39 topographical information of rivers at a reach scale. Although attempts have been
40 made to measure the dynamic surface roughness pattern underwater (e.g. [1, 2]),
41 there is still a lack of real time airborne methods to measure the instantaneous surface
42 elevation with sub-millimeter accuracy and at a very high temporal resolution. This
43 information is of great importance for us to advance the existing theoretical link
44 between the free surface behaviour and the underlying turbulent flow structures
45 which carry information about the flow and sediment bed [3]. This link can be
46 used to study the changes in the turbulent flow structures and velocity depth profile
47 remotely for a range of open channel flows in the laboratory and in the field using an
48 array of acoustic sensors deployed on a large scale, e.g. with a swarm of unmanned
49 aerial vehicles (UAV).

50 The main focus of this paper is to present a new method based on acoustic
51 boundary integral equations and a pseudo-inverse technique applied to a matrix
52 based equation to recover the instantaneous elevation of a dynamically rough surface
53 at sub-millimeter accuracy, high temporal resolution and a representatively large
54 spatial scale. In particular, this approach enables us to study the acoustic scattering

55 from an inhomogeneous roughness that supports multiple scales.

56 The paper is organized in the following manner. Section II presents the underlying
57 theory of acoustic scattering. This theory is then used in combination with the matrix
58 inversion method which is described in Section III. Section IV presents the results
59 of the application of the proposed inversion method to the acoustic pressure data
60 which were predicted with the standard Kirchhoff approximation and with the Finite
61 Difference Time Domain (FDTD) method. The conclusions are drawn in Section V.

62 **II Scattering of acoustic waves from a rough sur-** 63 **face**

64 Let us consider a semi-infinite space in Cartesian coordinate system $Oxyz$ bounded
65 by rough surface S which mean plane S_0 coincide with Oxy coordinate plane. Spatial
66 scales and distribution of surface elevation $\zeta(x)$ are assumed to be arbitrary within
67 the validity range of the proposed method and in this paper both deterministic
68 and random profiles are tested. In order to simplify the numerical calculations, it
69 is assumed that the surface is uniform in Oy -direction and the acoustic source is a
70 directional line source which directivity pattern $A(x, z)$ is defined in Section IV. This
71 makes the stated problem one dimensional. The main axis of the far-field directivity
72 pattern is inclined at the angle ψ_0 with respect to the Ox axis and it is aligned with
73 the centre of coordinates. The coordinates of the source and receiver are defined
74 by (x_1, z_1) and (x_2, z_2) , respectively. The source emits a continuous harmonic wave
75 $\exp(-i\omega t)$ with angular frequency ω and constant amplitude in time.

76 In this paper the roughness is defined by the dynamic behaviour of the water flow
77 free surface. To maintain harmonic dependence on time, as suggested above, it is

78 assumed that the roughness is frozen over a short time period at which the complex
79 acoustic pressure of the scattered harmonic wave needs to be measured. This is true
80 because the speed of sound in air $c_0 = 340$ m/s is much faster than the maximum
81 phase velocity $U = U_0 + c_p$ at which the surface roughness pattern on the flow surface
82 of a typical shallow water river with the mean depth h will propagate, i.e. $c_0 \gg U$.
83 Here U_0 denotes the flow velocity and $c_p = \sqrt{gh}$ is the phase velocity of the gravity
84 waves, g is the gravity.

85 In this paper the scattering from a rough surface is approximated by the tan-
86 gent plane approximation as suggested in [4]. We assume that the surface is rigid
87 which is a good approximation for the case when sound propagates in air above a
88 dynamically rough water surface, e.g. free surface of a turbulent open channel flow.
89 The approximation is based on the Kirchhoff method and principles of geometrical
90 optics (e.g. [5]), and it is valid if local curvature radius a of the rough surface is
91 much greater than the acoustic wavelength $\lambda = 2\pi/k$, where k is wavenumber of the
92 acoustic wave. For the diffraction on a sphere, this condition can be stated in the
93 following form

$$\sin \psi \gg \frac{1}{(ka)^{1/3}}, \quad (1)$$

94 where a is a radius of the sphere locally inscribed in rough surface. The condition in
95 eq. (1) can be relaxed to [6]

$$\sin \psi > \frac{1}{(ka)^{1/3}}, \quad (2)$$

96 so that the Kirchhoff approach remains accurate for the incident angles far from the
97 low grazing angles. In this paper condition (2) is used in the numerical simulation
98 to define the surface.

99 Assuming that the distances from the source R_1 and receiver R_2 to a given point
100 on the mean surface (see Figure 1) are much greater than the acoustic wavelength

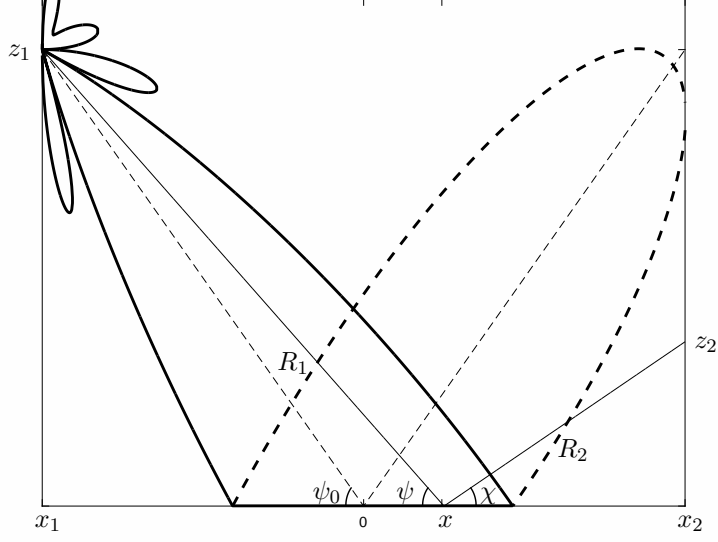


Figure 1: The geometry of the acoustic problem of rough surface scattering.

101 and using the Kirchhoff method, the scattered acoustic pressure can be approximated
 102 by [4, 7]

$$p(x_2, z_2) = -\frac{i}{2\pi k} \int_{S_0} \frac{A(x)}{\sqrt{R_1 R_2}} \exp [ik(R_1 + R_2) - iq_z \zeta(x)] \left[q_z - q \frac{\partial \zeta(x)}{\partial x} \right] dx, \quad (3)$$

where $\zeta(x)$ is surface elevation and

$$q_z = k \left(\frac{z_1}{R_1} + \frac{z_2}{R_2} \right), \quad (4)$$

$$q = -k \left(\frac{x_1 - x}{R_1} + \frac{x_2 - x}{R_2} \right), \quad (5)$$

$$R_1 = \sqrt{(x - x_1)^2 + z_1^2}, \quad (6)$$

$$R_2 = \sqrt{(x - x_2)^2 + z_2^2}. \quad (7)$$

103 Assuming that the surface is smooth, $\partial \zeta(x)/\partial x \ll 1$, equation (3) can be simplified

104 to

$$p(x_2, z_2) = -\frac{i}{2\pi k} \int_{S_0} \frac{A(x)}{\sqrt{R_1 R_2}} \exp [ik(R_1 + R_2) - iq_z \zeta(x)] q_z dx. \quad (8)$$

105 If the profile of the surface $\zeta(x)$ is known than the integral in equation (8) can be
106 solved numerically. However, the surface in the above integral is assumed to be
107 unknown and it is the acoustic pressure in the left hand side which is known from
108 experiments or from synthetic data (obtained with the Kirchhoff approximation and
109 FDTD method in this paper). This formulates an inversion problem where the
110 variable $\zeta(x)$ needs to be recovered from the available acoustic pressure data.

111 **III Matrix inverse method**

112 In order to invert the surface elevation $\zeta(x)$ it is proposed to use a numerical approach
113 to solve integral equation (8). For this purpose the integral is discretised over the
114 surface S_0 with the M uniform spatial elements $\Delta x = x_{m+1} - x_m$, $m = 1, \dots, M$
115 and approximated by the sum over these elements. It is noted that the size of the
116 element Δx has to be at least five times smaller than the acoustic wavelength λ [6]
117 (i.e. $\Delta x < \lambda/5$). The scattered acoustic pressure at the receiver position (x_2, z_2) can
118 be approximated by

$$p(x_2, z_2) = -\frac{i}{2\pi k} \sum_{m=1}^M \frac{A(x_m)}{\sqrt{R_{1,m} R_{2,m}}} \exp [ik(R_{1,m} + R_{2,m}) - iq_{z,m} \zeta(x_m)] q_{z,m} \Delta x, \quad (9)$$

119 where all the terms with the index m are defined at points x_m , $m = 1, \dots, M$ on the
120 surface S_0 . Equation (9) can be rewritten in the form of a scalar product of two
121 vectors

$$p(x_2, z_2) = \mathbf{D}_M \mathbf{E}_M, \quad (10)$$

where

$$\mathbf{D}_M = \left\{ -\frac{i}{2\pi k} \frac{A(x_m)}{\sqrt{R_{1,m}R_{2,m}}} \exp [ik(R_{1,m} + R_{2,m})] q_{z,m} \Delta x \right\}_{m=1,\dots,M}, \quad (11)$$

$$\mathbf{E}_M = \{\exp [-iq_{z,m}\zeta(x_m)]\}_{m=1,\dots,M}. \quad (12)$$

122 In order to retrieve the surface profile $\zeta(x)$ it is necessary to have acoustic pressure
 123 data recorded at more than one receiver positions that the acoustic pressure vector
 124 \mathbf{P} with N elements can be formed. With multiple receiver positions defined by the
 125 coordinates $(x_{2,n}, z_{2,n})$, $n = 1, \dots, N$, equation (10) needs to be converted into the
 126 matrix form in order to apply the matrix inversion.

127 One way of deriving the matrix form is to isolate the unknown elevation of the
 128 rough surface $\zeta(x)$ at the points x_m , $m = 1, \dots, M$ for all receiver positions in one
 129 single vector \mathbf{E}_M . In doing so it is assumed that for fixed index m the variability of
 130 $q_{z,mn}$, $n = 1..N$ with respect to the position on the surface is negligible in the vicinity
 131 of the specular point defined by the angle ψ_0 as shown in Figure 1. This gives

$$\mathbf{P}_{N \times 1} = \mathbf{H}_{N \times M} \mathbf{E}_{M \times 1}, \quad (13)$$

132 where the elements of the matrix $\mathbf{H}_{N \times M}$ are defined by

$$h_{mn} = \left\{ -\frac{i}{2\pi k} \frac{A(x_{mn})}{\sqrt{R_{1,mn}R_{2,mn}}} \exp [ik(R_{1,mn} + R_{2,mn})] q_{z,mn} \Delta x \right\}_{m=1,\dots,M,n=1,\dots,N} \quad (14)$$

133 and unknown vector $\mathbf{E}_{M \times 1}$ is given by equation (12) with $q_{z,m}$ defined by the receiver
 134 positioned at the specular angle ψ_0 . The form of equation (13) is identical to that
 135 used in inverse frequency response function (IFRF) techniques with $\mathbf{H}_{N \times M}$ repre-
 136 senting transfer matrix for an array of microphones and vector $\mathbf{E}_{M \times 1}$ representing
 137 velocity potentials on the surface [11]. This allows us to apply previously developed
 138 techniques to recover surface profile.

139 It is practical to assume that the number M of unknown points on the surface is
140 greater than the number of receivers N ($M > N$). However, this leads to an under-
141 determined system of equations which may result in an ill-conditioned matrix and a
142 non-unique inverse solution to problem stated in equation (13). In order to invert
143 the matrix $\mathbf{H}_{N \times M}$ in equation (13) it is proposed to use a pseudo-inverse method
144 based on the singular value decomposition technique (SVD) (e.g. [8]). Applied to
145 matrix $\mathbf{H}_{N \times M}$ this gives

$$\mathbf{H}_{N \times M} = \mathbf{U}_{N \times N} \mathbf{S}_{N \times M} \bar{\mathbf{V}}_{M \times M}^T, \quad (15)$$

146 where $\mathbf{U}_{N \times N}$ and $\mathbf{V}_{M \times M}$ are unitary matrices (defined by $\mathbf{A} \bar{\mathbf{A}}^T = \mathbf{I}$), $\mathbf{S}_{N \times M}$ is
147 a diagonal matrix with nonnegative elements arranged in the descending order of
148 smallness, $\bar{\mathbf{A}}$ stands for complex conjugate and \mathbf{A}^T denotes matrix transpose. In
149 order to apply pseudo-inverse techniques and decrease the computational time, in
150 this paper the truncated form of matrices \mathbf{S} and \mathbf{V} in equation (15) was used so that

$$\mathbf{H}_{N \times M} = \mathbf{U}_{N \times N} \mathbf{S}_{N \times N} \bar{\mathbf{V}}_{N \times M}^T. \quad (16)$$

151 Applying the SVD to equation (13) and using the definition of the unitary matrix
152 the unknown vector $\mathbf{E}_{M \times 1}$ can be expressed in the following form

$$\mathbf{E}_{M \times 1} = \mathbf{V}_{M \times N} \mathbf{S}_{N \times N}^{-1} \bar{\mathbf{U}}_{N \times N}^T \mathbf{P}_{N \times 1}, \quad (17)$$

153 where $\mathbf{S}_{N \times N}^{-1}$ indicates the matrix inverse. The matrix $\mathbf{S}_{N \times N}$ may contain small
154 order elements resulting in singular values in the inverted matrix $\mathbf{S}_{N \times N}^{-1}$. In order to
155 regularize ill-conditioned matrix and to filter the singular elements from the inverse
156 matrix it is proposed to use the Tikhonov regularization technique (e.g. [11] and [9])
157 that gives

$$\mathbf{E}_{M \times 1} = \mathbf{V}_{M \times N} \mathbf{S}_{\beta, N \times N}^{-1} \bar{\mathbf{U}}_{N \times N}^T \mathbf{P}_{N \times 1}, \quad (18)$$

158 where $\mathbf{S}_{\beta, N \times N}^{-1} = [\mathbf{S}_{N \times N} + \beta^2 \mathbf{S}_{N \times N}^{-1}]^{-1}$ and β is the regularization parameter. In or-
 159 der to adjust parameter β we used the generalised cross validation (GCV) technique.
 160 This technique requires to minimize the following function

$$F(\beta) = \frac{r_\beta^2}{\text{Tr} \left(\mathbf{I}_{N \times N} - \mathbf{U}_{N \times N} \mathbf{S}_{N \times N} \mathbf{S}_{\beta, N \times N}^{-1} \bar{\mathbf{U}}_{N \times N}^T \right)^2}, \quad (19)$$

161 in which r_β is the residue defined by l^2 -vector norm

$$r_\beta = \left\| \left(\mathbf{I}_{N \times N} - \mathbf{U}_{N \times N} \mathbf{S}_{N \times N} \mathbf{S}_{\beta, N \times N}^{-1} \bar{\mathbf{U}}_{N \times N}^T \right) \mathbf{P}_{N \times 1} \right\|. \quad (20)$$

162 The argument (phase) of each element of vector $\mathbf{E}_{M \times 1}$ provides information about
 163 the surface elevation. In order to retrieve the phase from matrix equation (18)
 164 the complex natural logarithm is applied element-wise to the results of the matrix
 165 product. This yields

$$\mathbf{Q}_{\zeta_{M \times 1}} = -\Im[\text{Ln}(\mathbf{E}_{M \times 1})], \quad (21)$$

166 where

$$\mathbf{Q}_{\zeta_{M \times 1}} = \{q_{z,m} \zeta(x_m)\}_{m=1, \dots, M}, \quad (22)$$

167 with $\Im(\langle \cdot \rangle)$ representing the imaginary part of the natural logarithm. It is noted
 168 that the application of Ln in equation (21) is restricted to the case when $-\pi <$
 169 $q_{z,m} \zeta(x_m) < \pi$ that enables us to uniquely define the elements of the vector $\mathbf{Q}_{\zeta_{M \times 1}}$.
 170 This condition holds in the vicinity of a specular point defined by the angle ψ_0
 171 and fails as distance between specular point and x_m , $m = 1, \dots, M$ increases. The
 172 discretized roughness profile $\{\zeta_m\}$ at the points $\{x_m\}$ can then be deduced as

$$\{\zeta_m\}_{m=1, \dots, M} = \left\{ \frac{-\Im[\text{Ln}(e_m)]}{q_{z,m}} \right\}_{m=1, \dots, M}, \quad (23)$$

173 where e_m is an element of the vector $\mathbf{E}_{M \times 1}$.

174 The fact that the proposed inversion largely depends on the proximity of a surface
 175 point to the specular point leads to the idea of replacing the directional source with
 176 simple monopole with a unit amplitude. As a result, the elements of the matrix
 177 $\mathbf{H}_{N \times M}$ can be simplified to

$$h_{mn} = \left\{ -\frac{i}{2\pi k} \frac{\exp [ik(R_{1,mn} + R_{2,mn})]}{\sqrt{R_{1,mn}R_{2,mn}}} q_{z,mn} \Delta x \right\}_{m=1,\dots,M,n=1,\dots,N}. \quad (24)$$

178 This reduces input data to geometrical parameters defined by the position of source
 179 and receivers with respect to the surface S_0 and data recorded on the array of re-
 180 ceivers.

181 IV Results

182 In this paper, validation of the proposed inversion method (equation (23)) is based on
 183 two sets of synthetic data generated using the Kirchhoff integral and FDTD method.
 184 The former demonstrates the implementation of the proposed inverse technique and
 185 the latter shows application of this technique to independent set of data obtained in
 186 order to retrieve unknown surface profile.

187 A Simulated roughness

188 In this section the acoustic pressure scattered by the rough surface was modelled with
 189 the Kirchhoff integral (equation (8)). In order to reconstruct the surface elevation it
 190 was proposed to use an array of $N = 121$ receivers arranged on a circular arch with the
 191 radius of $R = 0.4$ m as illustrated in Figure 2. The receivers and source are positioned
 192 on the opposite sides of the arch. The arch is suspended at $d = 0.01$ m above the
 193 mean surface of water, S_0 , and the centre of the arch coincides with the centre of

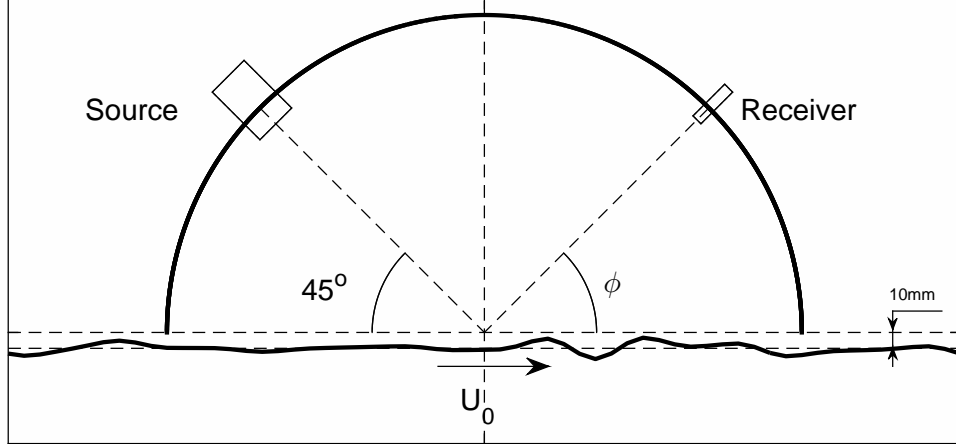


Figure 2: The acoustic setup used to reconstruct the rough surface in the numerical experiment.

194 Ox axis. The source was installed at the angle of $\psi_0 = 45^\circ$ and its coordinates were
 195 $(R \cos \psi_0, R \sin \psi_0 + d)$, where d is the vertical distance of the circular arch base to
 196 the plane S_0 . The position of receivers is defined by $(-R \cos \phi, R \sin \phi + d)$, where ϕ
 197 varies from 15° to 75° with 0.5° resolution that produces 121 receiver positions. The
 198 sound source emitted a continuous harmonic wave at $f = 43$ kHz and its far-field
 199 directivity pattern was defined by

$$A(\theta) = \frac{J_1(ka \sin \theta)}{ka \sin \theta}, \quad (25)$$

200 where $a = 0.02$ m is the radius of the source aperture. The position of the receivers
 201 was characterized by the angle ϕ which was taken from the horizontal line. The
 202 number of the receivers in the array, N , and the adopted geometry were consistent
 203 with that used in the experiments reported by Nichols [10]. Increasing the number
 204 of receivers may result in more singular values and it may lead to a more unstable
 205 inverse solution. Decreasing the number of the receivers may lead to a poorer spatial
 206 resolution of the surface elevation and higher ambiguity.

207 In the calculations reported in this section the 1-D rough surface $\zeta(x)$ was sim-
 208 ulated with the Fourier series containing random phase and amplitudes assigned in
 209 accordance with the typical characteristics of gravity-capillary waves [12]. This gives

$$\zeta(x) = \sigma \sum_n C_n \cos(K_n x + \tau_n), \quad (26)$$

210 where σ is the standard deviation of the rough surface elevation (mean roughness
 211 height), K_n is wavenumber in the surface roughness spatial spectrum, τ_n is phase
 212 which value is randomly generated and amplitude C_n is defined by the correlation
 213 function of the waves of which the surface roughness pattern is composed and it is
 214 proportional to the wavelength l_n of the n -th harmonic in the Fourier expansion so
 215 that

$$C_n \sim \left(\frac{2\pi}{l_n}\right)^{\alpha/2}. \quad (27)$$

216 In particular the amplitude of each term in the Fourier expansion is linked to the
 217 power spectrum slope defined by the power of $\alpha = -4$ [13]. The surface elevation
 218 constructed with this kind of spatial spectrum supported multiple scales ranging
 219 from 8 mm to 115 mm and satisfied the condition (2) on the validity of Kirchhoff
 220 approximation. The standard deviation of the surface is set to $\sigma = 1$ mm.

221 Figure 3(a) shows the surface elevation simulated with the Fourier series using
 222 the range of spatial wavelengths of $8\text{mm} < l_n < 115$ mm and compared with surface
 223 elevation reconstructed with the proposed inversion method. This figure also shows
 224 the absolute error in the surface reconstruction which was calculated as $\epsilon_\zeta(x) =$
 225 $|\zeta_p(x) - \zeta_s(x)|$, where $\zeta_p(x)$ is the surface elevation predicted with the inverse method
 226 and $\zeta_s(x)$ is the surface elevation simulated with equation (26). The inversion was
 227 applied to the surface interval containing $M = 3000$ surface points that included the
 228 specular reflection point and its vicinity. It can be seen from the data presented in
 229 Figure 3 that the range of x for which the surface roughness reconstruction could be

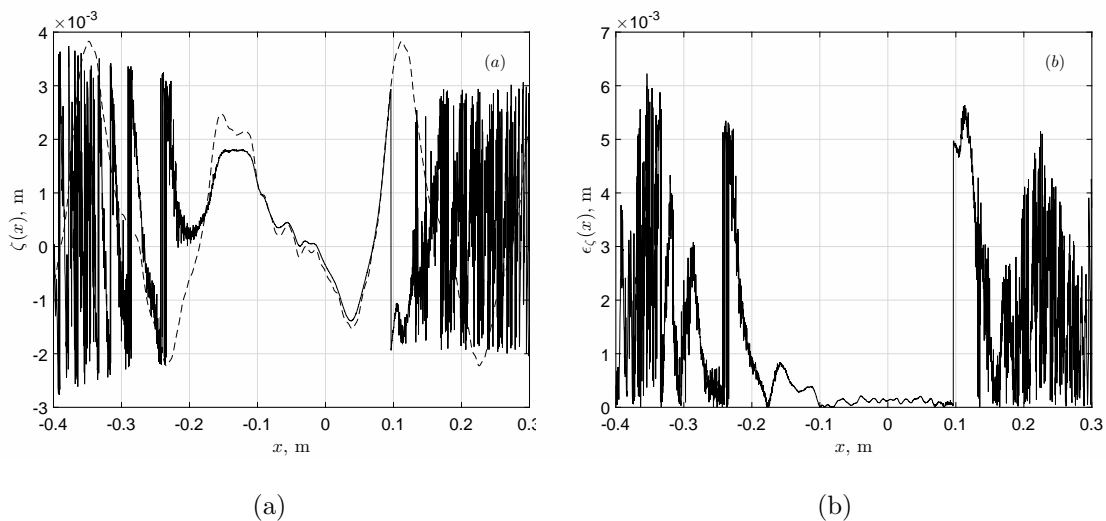


Figure 3: (a) An example of the surface realization, $\zeta(x)$, (dashed line) used in equation (8) and its reconstruction from the Kirchhoff approximation (solid line) based on equation (23). (b) Absolute error of the reconstructed surface.

230 achieved was limited by the position of the specular reflection point which was in the
 231 range of $-0.1 \text{ m} < x < 0.1 \text{ m}$. In particular, this is illustrated in Figure 3(b) where the
 232 absolute error of the surface reconstructed within this interval is limited and does not
 233 exceed 0.22 mm which is considerably smaller than the maximum roughness height
 234 of 2.5 mm . The root mean square (RMS) error for this range does not exceed 0.12
 235 mm that is 12% of the true mean roughness height. In this analysis the root mean
 236 square error was calculated as

$$\epsilon_{\text{rms}} = \sqrt{\frac{1}{N} \sum_{n=1}^N [\zeta_p(x_n) - \zeta_s(x_n)]^2}, \quad (28)$$

237 where the deduced surface elevation $\zeta_p(x_n)$ and simulated surface elevation $\zeta_s(x_n)$
 238 are taken at the point x_n . It is noted that these errors are comparable or smaller to
 239 those which are typical for an alternative laser-induced fluorescence (LIF) method

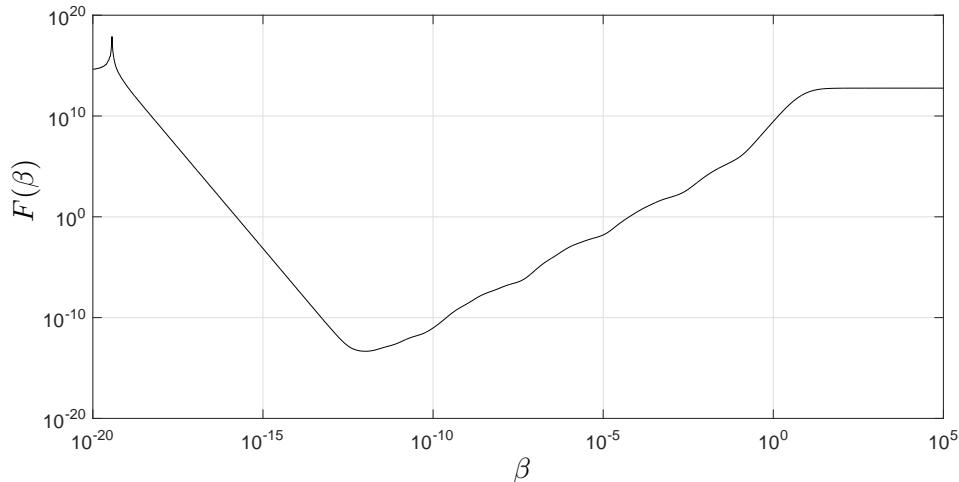


Figure 4: An example of the behaviour of the function $F(\beta)$ for the range of $10^{-20} < \beta < 10^5$.

240 (e.g. ± 0.14 mm for the LIF method used in ref. [10]).

241 The regularization parameter β was selected in accordance with equation (19).
 242 Figure 4 illustrates the variation of the GCV function F for the reconstruction process
 243 for the surface shown in Figure 3(a). The parameter β is small ($\beta \sim 10^{-12}$) and
 244 defines the threshold below which equation (18) becomes unstable. It increases with
 245 the decrease in the number of receivers causing the inversion process to become more
 246 unstable.

247 In order to understand the range of scales which can be recovered with equation
 248 (18) we compared the power spectrum of the surface roughness for a representative
 249 number of realizations obtained by varying randomly phase with the amplitudes
 250 of the Fourier expansion (equation (26)). The power spectrum was calculated by
 251 applying the Hanning window and Fourier transform to the original and recovered
 252 surface elevation data for each of the surface realization. It was then averaged over
 253 all the surface realizations. It was found that the average power spectrum converges

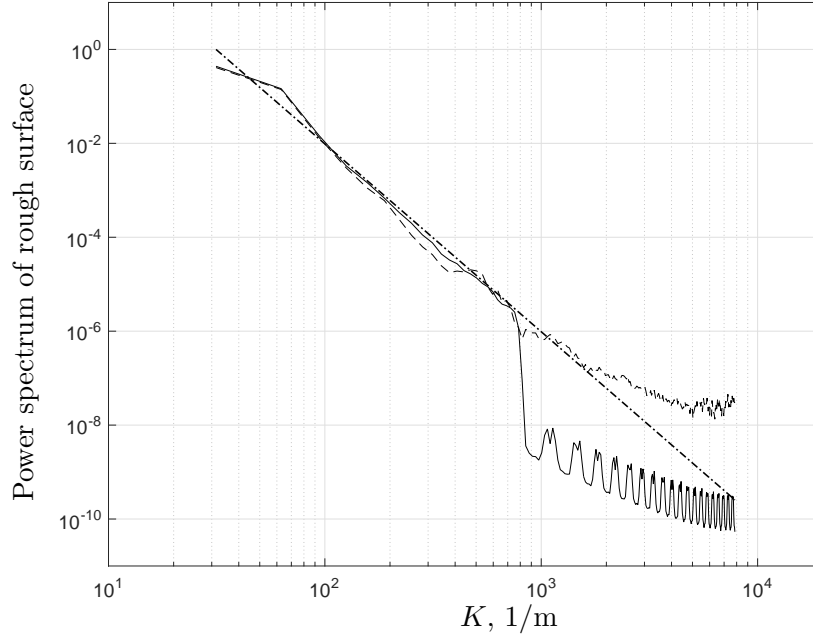


Figure 5: The normalized power spectrum averaged over 100 surface elevation realizations. Dash-dot line - the spectrum based on equation (27); dashed line - the inverted spectrum; solid line - the spectrum of the surfaces generated with equation (26).

254 to the true mean value to within 1% provided that at least 100 surface realizations
 255 were used. The average power spectrum inverted with the proposed method follows
 256 the slope $\alpha = -4$ defined by equation (27) for $K < 800$ 1/m (Figure 5). This
 257 corresponds to the lowest scale present in the simulated surface roughness wavelength
 258 of $l_n \approx 8$ mm. For the spectrum of larger scales (centimetre scale) when $K < 800$
 259 the agreement between the average spectrum inverted with the proposed technique
 260 and that defined by equation (26) was within 15%.

261 **B Measured roughness**

262 In order to illustrate the application of the inversion method developed in Section III
263 we used the acoustic pressure data $\mathbf{P}_{N \times 1}$ calculated with the Kirchhoff approximation
264 and with the full-wave 2-D FDTD method [14] for a range of roughness realizations
265 measured with the light-induced fluorescence method detailed in [10]. In the case of
266 the Kirchhoff approximation the acoustic pressure was calculated as described in the
267 previous section.

268 In the case of the FDTD method the acoustic pressure was computed for a source
269 with directivity pattern defined by (25). This source directivity was simulated by
270 setting up a 33 mm long line array of 49 point sources operated in phase. The
271 frequency of the acoustic wave emitted by the source was $f = 43$ kHz. The time and
272 space discretization intervals in the FDTD calculations were $1.03 \mu\text{s}$ and 0.5 mm,
273 respectively [15].

274 The surface roughness data used in this work were obtained in a hydraulic flume
275 with the method detailed in [10] and these were assumed to be exact in our calcu-
276 lations. The flume had a bed of hexagonally packed spheres with a diameter of 25
277 mm, and was tilted to a slope of $S_0 = 0.004$. The flow was turbulent, uniform and
278 constant velocity was maintained across the length of the measured spatial interval.
279 The surface elevation data was collected for four flow regimes which corresponded to
280 the flow with the 60, 70, 80 and 90 mm of uniform water depth, respectively. These
281 regimes corresponded to the mean flow velocity of 0.43, 0.50, 0.57 and 0.65 m/s,
282 respectively. The arrangement of the receiver positions in the models was identical
283 to that detailed in the previous section for a given realization of $\zeta(x)$.

284 In Figure 6 the real and imaginary parts of the angular dependent acoustic pres-
285 sure predicted with the FDTD method is compared against that predicted with the

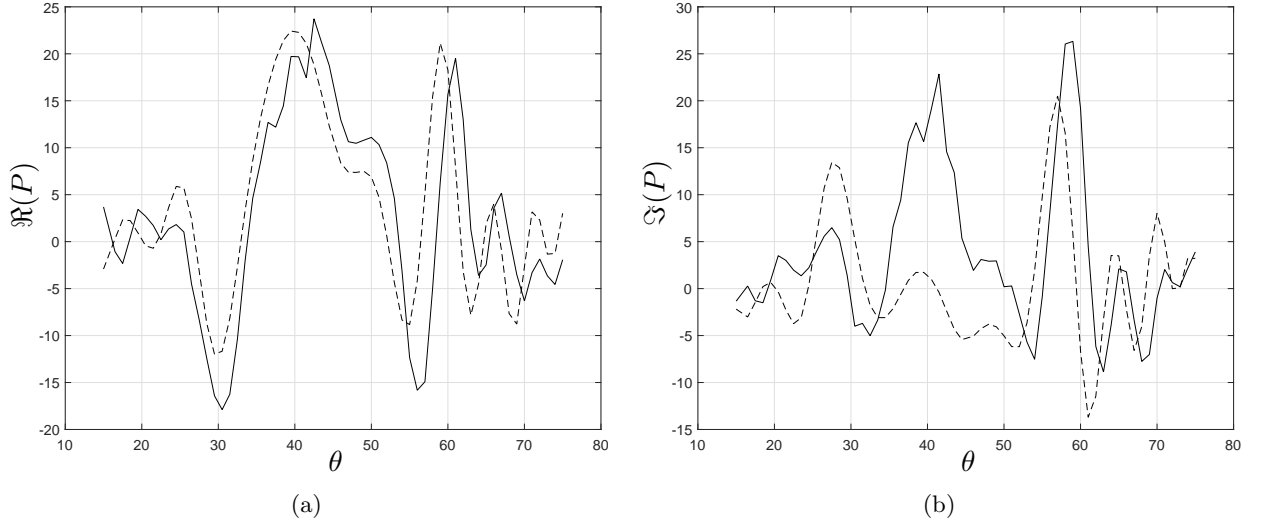


Figure 6: The scattered acoustic pressure for a single realization of the rough surface elevation for flow depth 60 mm predicted with FDTD method (solid line) and Kirchhoff approximation (8) (dashed line). (a) Real part, (b) imaginary part.

286 Kirchhoff approximation (8). These results correspond to a realistic flow surface
 287 roughness realization measured for the 60 mm deep flow regime. The results suggest
 288 that the Kirchhoff approximation generally underpredicts the acoustic pressure in
 289 comparison to that predicted by the FDTD method. This is particularly notice-
 290 able in the case of the imaginary part and for the angles of incidence close to 45° .
 291 These acoustic pressure data were then used with the proposed inversion technique
 292 to reconstruct the flow surface roughness.

293 Figures 7 (a)-(d) present the results of the application of the inverse technique
 294 to the acoustic pressure data predicted with the Kirchhoff approximation and with
 295 the FDTD method for flow surface realizations representing each of the four flow
 296 regimes. The inversion results are shown in the range $-0.1 < x < 0.1$ m where the
 297 maximum relative error was within 45% when the acoustic pressure was predicted

298 with the FDTD method and 20% when the acoustic pressure was predicted with the
299 Kirchhoff approximation. Within this interval the effects of shadowing and multiple
300 scattering are relatively small that enables us to use equation (8) as an accurate
301 approximation to the full-wave FDTD results. In all cases the minimum of β was
302 in the interval $[0, 1]$ and its values is listed in Table 1. The accuracy we achieved
303 depended on how far the point on the surface was from the nominal specular reflection
304 point.

305 Figure 8 presents the mean spatial spectra which demonstrate the range of scales
306 of roughness which were recovered through the proposed inversion technique. These
307 spectra were inverted using the acoustic pressure data predicted with the Kirchhoff
308 approximation and with the FDTD method. As it was noted in the previous section
309 IV A, the normalized power spectrum provides information on the contribution of
310 different roughness scales to the pattern of waves observed on the surface. For the
311 four flow regimes considered in this work the recovered surface predicts the actual
312 slope of the power spectrum closely for $K < 1000$ 1/m. However, it is clear that
313 the accuracy of the proposed inversion techniques deteriorates as K approaches 1000
314 1/m that limits the use of the technique to identify the correct range of roughness
315 scales, i.e. those scales which are at a $l_n < 6.3$ mm spatial wavelength. This can
316 be explained by the limitations of the Kirchhoff approximation (equation (8)) as the
317 local radius of curvature increases with the decrease of the surface scales. It is also
318 noted that, although in this paper the coordinates of the receivers are exact, the
319 implementation of the method can be limited by the uncertainties in the receiver
320 positions. The sensitivity of the proposed method is analysed on Appendix A.

321 It is difficult to obtain a useful measure of the error between the measured spec-
322 trum and that reconstructed with the proposed inversion method by comparing these
323 spectra directly. This is because the spectral power shown in Figure 8 varies by 10

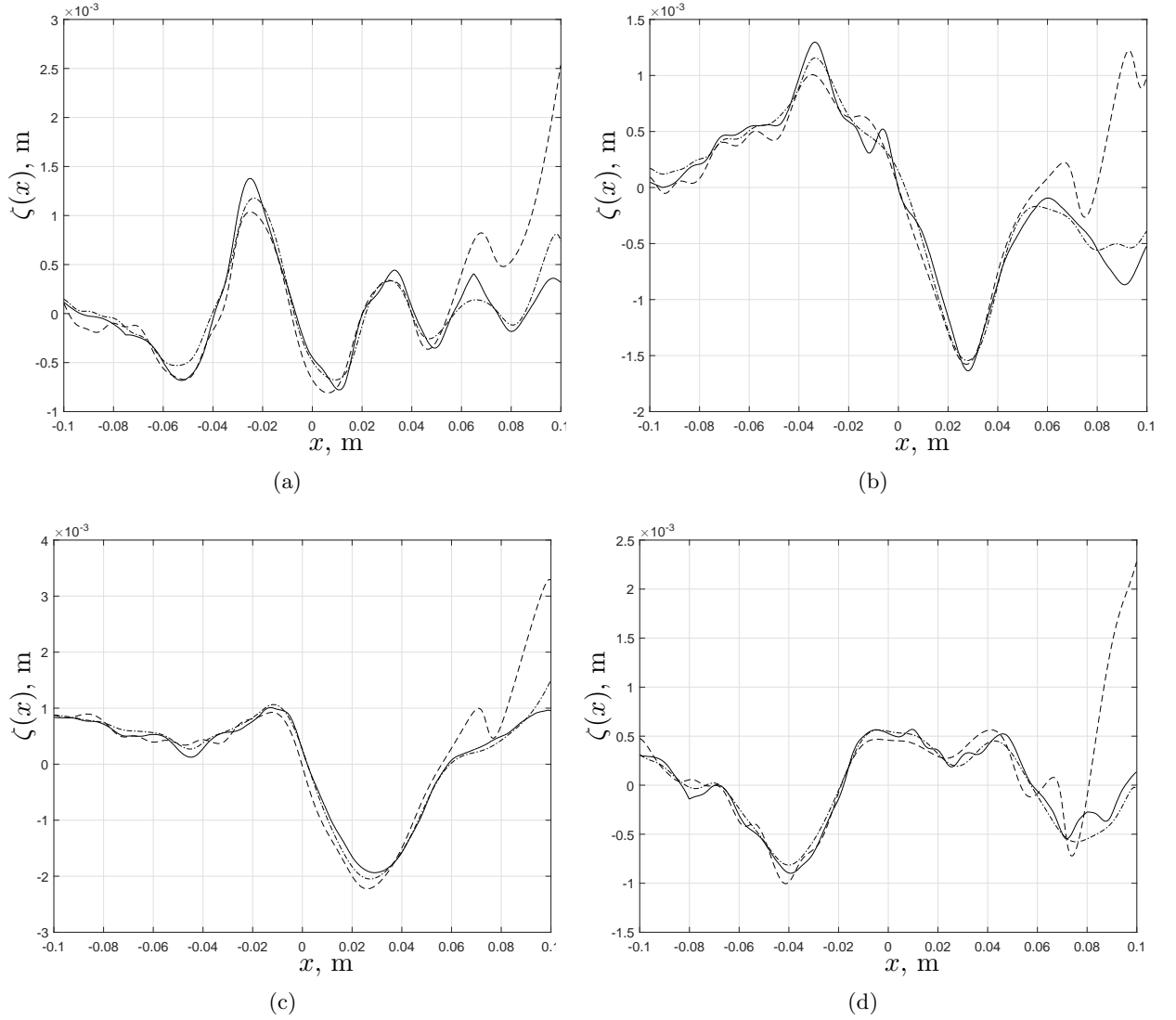


Figure 7: Examples of the surface elevation $\zeta(x)$ for the four flow regimes. Solid line - measured with the LIF method; dashed line - reconstructed with the sound pressure data predicted with the FDTD mode; dashed-dot line - reconstructed with the acoustic pressure data predicted with the Kirchhoff approximation. (a) Flow depth 60 mm, (b) flow depth 70 mm, (c) flow depth 80 mm, (d) flow depth 90 mm.

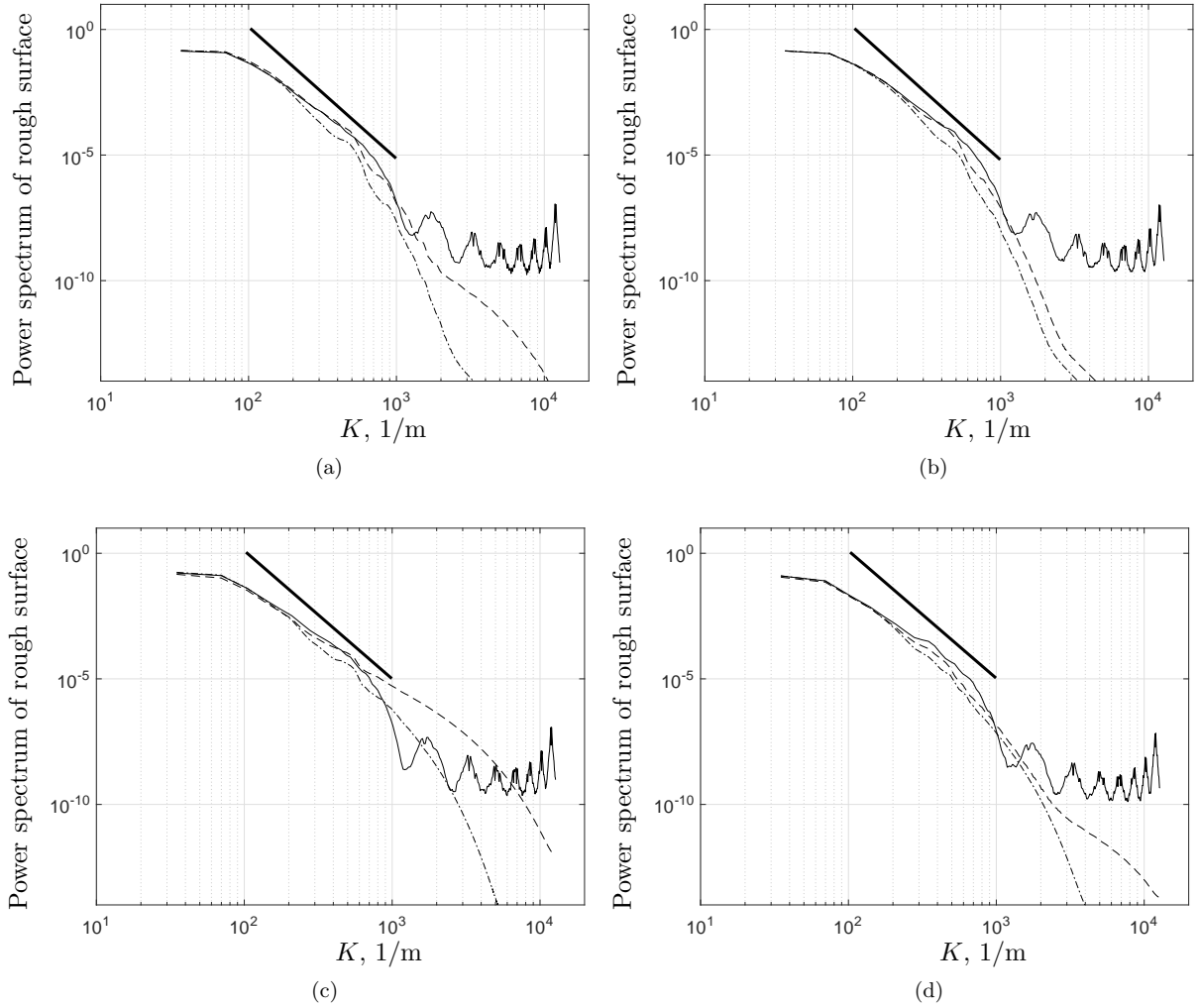


Figure 8: The normalized power spectrum of rough surface (solid line) compared against the power spectrum of the reconstructed surface where dashed and dashed-dot lines represent the use of FDTD and Kirchhoff approximation data, respectively. Thick solid line represents slope of the reconstructed power spectrum. (a) Flow depth 60 mm, (b) Flow depth 70 mm, (c) Flow depth 80 mm, (d) Flow depth 90 mm.

324 orders of magnitude over the considered range of wavenumbers. For this purpose
325 all results in Figure 8 are compared against slope of the measured surface which is
326 deduced with the linear regression technique between $K > 100$ and $K < 1000$ 1/m.
327 The slope of the measured power spectrum for all flow regimes is approximated by
328 $\alpha = -5$. A comparison between fitted line with slope -5 and spectra recovered with
329 the proposed acoustic method suggests that the method provides adequate prediction
330 of the surface power spectrum.

331 **V Conclusion**

332 In this paper we demonstrate the derivation of an inversion method based on the
333 Kirchhoff approximation of the boundary integral equation and the application of an
334 inverse technique based on SVD and Tikhonov regularization to an underdetermined
335 system of equations. The surface roughness data we used in our work were simulated
336 surface roughness and surface roughness measured with the LIF method that were
337 assumed to be exact. The proposed inversion method enables us to determine the
338 1-D surface roughness with a maximum RMS error of 45% (FDTD method) and 20%
339 (Kirchhoff approximation), both being sub-millimeter scale errors. This method also
340 enables us to estimate the average spatial power spectrum of the surface roughness for
341 the range of wavenumbers $K < 1000$ 1/m. This corresponds to spatial wavelengths
342 of $l_n > 6.3$ mm. For the simulated surface roughness this spectrum converges to its
343 true mean value to within 15% provided that at least 100 realizations are used in
344 the averaging process. The area of the rough surface which can be reconstructed
345 with the proposed acoustic setup and with the reported accuracy is within ± 0.1 m
346 range. This range determines the maximum wavelength in the spatial spectrum of
347 surface which can be estimated with the proposed acoustic setup and it is limited

348 by the wavelength of the incident acoustic waves, by the number and arrangement
349 of the receivers in the microphone array and by the adopted directivity of the sound
350 source. It is shown that the reconstructed surface roughness power spectrum follow
351 a power law characterising the simulated/measured surfaces.

352 The inversion method requires further improvements to increase accuracy for the
353 scales in the centimeter and sub-centimeter range of spatial wavelength. This should
354 involve the use of an extension of Kirchhoff approximation which can account for
355 higher roughness slopes or a more refined 3D numerical model for 2D roughness.
356 The retrieved roughness profiles can be used to find key statistical and spectral
357 characteristics of the water surface. The proposed method can potentially be used
358 together with the acoustic array measurements to accurately retrieve the temporal
359 and spatial profile of the dynamic shallow water flow.

360 **Acknowledgments**

361 The authors are grateful to Dr. Andrew Nichols (University of Sheffield) for the
362 provision of the LIF data some of which we used for the analysis reported in Section
363 IV B. The authors would like to thank unanimous reviewer of this paper for valuable
364 comments and suggestions.

365 **Appendix A: Sensitivity**

In order to test the sensitivity of the proposed inverse method it is necessary to simulate some type of geometrical uncertainty. In the case when position of all receivers are fixed the uncertainty in position is linked to the coordinates of the array frame. In this paper the frame is circular arch with radius $R = 0.4$ m. For

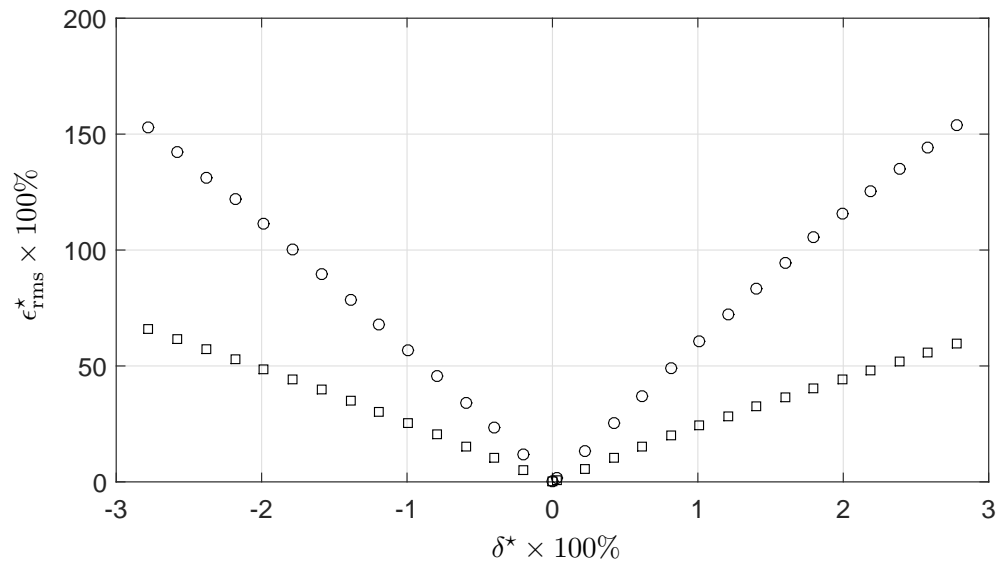


Figure 9: The relative variation in the RMS surface roughness height reconstructed for a given uncertainty in the x (squares) and z -coordinates (circles) for the receiver position

the 1D surface roughness the coordinates of the array frame can be varied along Oz and Ox axis. Introducing a small perturbation $\delta = \delta^* R$, where δ^* is dimensionless small parameter, to the distances R_1 and R_2 shown in equations (6) and (7) the uncertainty along Ox axis can be defined by

$$R_1 = \sqrt{(x - x_1 + \delta)^2 + z_1^2}, \quad (29)$$

$$R_2 = \sqrt{(x - x_2 + \delta)^2 + z_2^2}. \quad (30)$$

whereas the uncertainty along Oz axis is given by

$$R_1 = \sqrt{(x - x_1)^2 + (z_1 + \delta)^2}, \quad (31)$$

$$R_2 = \sqrt{(x - x_2)^2 + (z_2 + \delta)^2}. \quad (32)$$

366 In both cases dimensionless parameter δ^* varies within 3% of frame radius R around
 367 frame initial coordinates. The results are shown in Figure 9 where the uncertainty
 368 is introduced in the inversion with the FDTD simulation of acoustic scattering. It is
 369 observed that the variation along the Oz axis depicted in circles results in a higher
 370 relative deviation in the RMS roughness height defined by

$$\epsilon_{\text{rms}}^*(\delta^*) = \frac{\sqrt{\sum_{n=1}^N [\zeta_p(x_n, \delta^*) - \zeta_p(x_n, \delta^* = 0)]^2}}{\sqrt{\sum_{n=1}^N [\zeta_p(x_n, \delta^* = 0)]^2}}, \quad (33)$$

371 within which ζ_p represents the predicted surface roughness with the inverse method.
 372 The root mean square (RMS) roughness height reconstructed in the $[-0.1, 0.1]$ m
 373 spatial interval deviates linearly from the predicted initial ($\delta = 0$) RMS roughness
 374 height as the position of the frame varies within 3% from the initial position. The
 375 uncertainty in Ox coordinate of the frame $\delta^* \times 100\% = \pm 1\%$ with respect to its
 376 radius R results in 25% variation in the RMS roughness height. Applying the same

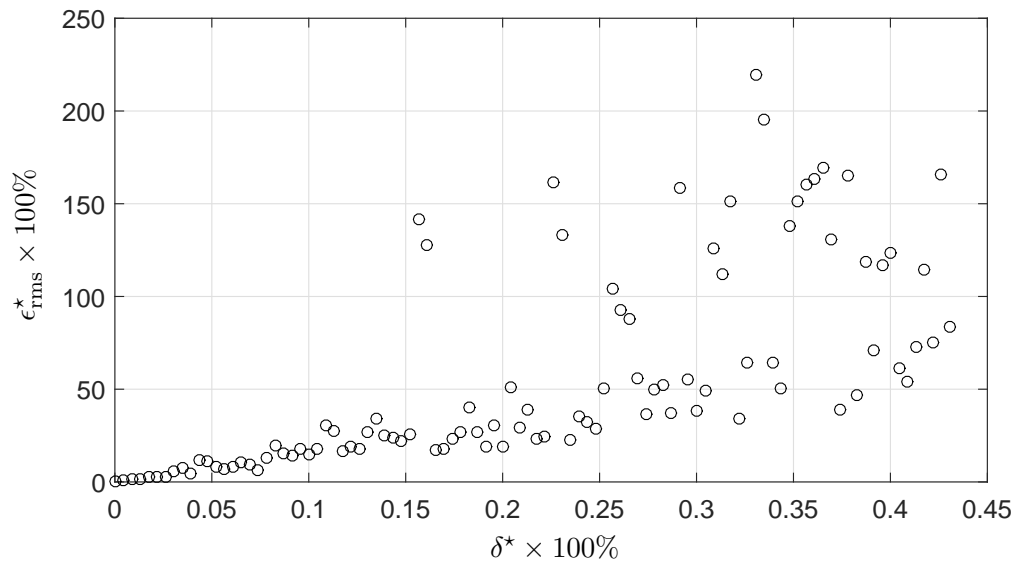


Figure 10: Relative variation in RMS surface roughness height computed for randomly perturbed positions of the receivers

377 uncertainty to the z coordinate of the receiver position results in approximately 50%
 378 deviation in the RMS roughness height from the initial solution.

379 To test the uncertainty in the receiver position it is proposed to introduce a ran-
 380 dom perturbation. The coordinates of all the 121 receivers are perturbed randomly
 381 with a uniform distribution in the circle which radius δ^* does not exceed half of the
 382 distance between two adjacent receivers which is approximately 3 mm. The results
 383 are shown in Figure 10. It is suggested that increasing the radius of the perturbation
 384 results in a significant increase in the variation of the RMS roughness height calcu-
 385 lated with equation (33). For 0.1% uncertainty in the position of each sensor the
 386 relative variation of the RMS roughness height is below 20% whereas at uncertainty
 387 approaching 0.5% (i.e. receiver is randomly positioned in the circle with radius ap-
 388 proaching 1.5 mm) of frame radius R the relative variation $\epsilon_{\text{rms}}^* \times 100\%$ is above 50%

389 that makes the inverse method invalid for reconstruction of roughness in the given
390 spatial interval. It is clear that method is 10 times more sensitive to the uncertainty
391 in the individual position of each receiver in the array compared to the uncertainty
392 in the position of the whole array.

393 **References**

- 394 [1] R.J. Wombell and J.A. DeSanto, "The reconstruction of shallow rough-surface
395 profiles from scattered field data," *Inverse Problems*, 7, 7–12 (1991).
- 396 [2] S.P. Walstead and G.B. Deane, "Reconstructing surface wave profiles from re-
397 flected acoustic pulses," *J. Acoust. Soc. Am.*, 133, 2597–2611 (2013).
- 398 [3] K. V. Horoshenkov, A. Nichols, S. J. Tait, G. A. Maximov, The pattern of
399 surface waves in a shallow free surface flow, *J. Geoph. Res.*, 118, 1864-1876
400 (2013).
- 401 [4] A. Krynkin, K. V. Horoshenkov, A. Nichols and S. J. Tait, "A non-invasive
402 acoustical method to measure the mean roughness height of the free surface of a
403 turbulent shallow water flow," *Review of Scientific Instruments*, 85 (11), 114902,
404 (2014).
- 405 [5] A. Ishimaru, *Wave Propagation and Scattering in Random Media* (Academic
406 Press, Inc., New York, 1978), pp. 484–487.
- 407 [6] E.I. Thorsos, "The validity of the Kirchhoff approximation for rough surface
408 scattering using a Gaussian roughness spectrum," *J. Acoust. Soc. Am.*, 83, 78–
409 92 (1988).

- 410 [7] F. G. Bass and I. M Fuks, *Wave Scattering from Statistically Rough Surfaces*
411 (Pergamon Press, Ltd, Oxford, 1979), p. 228.
- 412 [8] W. H. Press, S. A. Teukolsky, W. T. Vetterling and B. P. Flannery, *Numerical*
413 *Recipes: The Art of Scientific Computing* (3rd Edition, Cambridge University
414 Press, Cambridge, 2007), pp. 65–75.
- 415 [9] H.W. Engl, M. Hanke and A. Neubauer, *Regularization of Inverse Problems*,
416 (Kluwer Academic Publ., Dordrecht, 2000), pp. 221–237.
- 417 [10] A. Nichols, *The Interaction Mechanism of Airborne Acoustic Fields with Turbu-*
418 *lent Shallow Flows* (Ph.D. thesis, University of Bradford, UK, 2014), pp. 76–79.
- 419 [11] Q. Leclère, "Acoustic imaging using under-determined inverse approaches: Fre-
- 420 quency limitations and optimal regularization", *J. Sound Vib.*, 321, 605–619,
421 (2009).
- 422 [12] J.A. Toporkov and G.S. Brown, "Numerical Simulations of Scattering from
- 423 Time-Varying, Randomly Rough Surfaces", *IEEE T. Geosci. Remote*, 38, 1616–
424 1625 (2000).
- 425 [13] O. M. Phillips, "On the generation of waves by turbulent wind," *J. Fluid Mech.*,
426 2, 417–445 (1957).
- 427 [14] T. Van Renterghem, "Efficient outdoor sound propagation modeling with the
- 428 finite-difference time-domain (FDTD) method: a review," *Int. J. Aeroacoustics*,
429 13 (5-6), 385–404 (2014).
- 430 [15] K. V. Horoshenkov, T. Van Renterghem, A. Nichols and A. Krynkina, "Finite
- 431 difference time domain modelling of sound scattering by the dynamically rough
- 432 surface of a turbulent open channel flow," *Applied Acoustics*, 110, 13–22 (2016)

Table 1: Examples of the minimum values of the regularization parameter β obtained for 4 realizations of the surface elevation associated with the four adopted flow regimes.

	60 mm	70 mm	80 mm	90 mm
$\beta \times 10^7$	8.4	8.4	8.4	13

434 **List of Figures**

435 1 The geometry of the acoustic problem of rough surface scattering. 5

436 2 The acoustic setup used to reconstruct the rough surface in the nu-
437 merical experiment. 11

438 3 (a) An example of the surface realization, $\zeta(x)$, (dashed line) used
439 in equation (8) and its reconstruction from the Kirchhoff approxima-
440 tion (solid line) based on equation (23). (b) Absolute error of the
441 reconstructed surface. 13

442 4 An example of the behaviour of the function $F(\beta)$ for the range of
443 $10^{-20} < \beta < 10^5$ 14

444 5 The normalized power spectrum averaged over 100 surface elevation
445 realizations. Dash-dot line - the spectrum based on equation (27);
446 dashed line - the inverted spectrum; solid line - the spectrum of the
447 surfaces generated with equation (26). 15

448 6 The scattered acoustic pressure for a single realization of the rough
449 surface elevation for flow depth 60 mm predicted with FDTD method(solid
450 line) and Kirchhoff approximation (8) (dashed line). (a) Real part, (b)
451 imaginary part. 17

452 7 Examples of the surface elevation $\zeta(x)$ for the four flow regimes. Solid
453 line - measured with the LIF method; dashed line - reconstructed with
454 the sound pressure data predicted with the FDTD mode; dashed-dot
455 line - reconstructed with the acoustic pressure data predicted with the
456 Kirchhoff approximation. (a) Flow depth 60 mm, (b) flow depth 70
457 mm, (c) flow depth 80 mm, (d) flow depth 90 mm. 19

458	8	The normalized power spectrum of rough surface (solid line) compared against the power spectrum of the reconstructed surface where	
459		dashed and dashed-dot lines represent the use of FDTD and Kirchhoff	
460		approximation data, respectively. Thick solid line represents slope of	
461		the reconstructed power spectrum. (a) Flow depth 60 mm, (b) Flow	
462		depth 70 mm, (c) Flow depth 80 mm, (d) Flow depth 90 mm.	20
463			
464	9	The relative variation in the RMS surface roughness height reconstructed for a given uncertainty in the x (squares) and z -coordinates	
465		(circles) for the receiver position	23
466			
467	10	Relative variation in RMS surface roughness height computed for randomly perturbed positions of the receivers	25
468			